Energy & Environmental Science

COMMUNICATION

View Article Online
View Journal | View Issue

Cite this: *Energy Environ. Sci.*, 2017, **10**, 924

Received 6th March 2017,
Accepted 24th March 2017

DOI: 10.1039/c7ee00628d

rsc.li/ees

Enhanced electrocatalytic activity *via* phase transitions in strongly correlated $SrRuO_3$ thin films†

Sang A Lee,‡[ab] Seokjae Oh,‡[a] Jae-Yeol Hwang,[cd] Minseok Choi,[ef] Chulmin Youn,[g] Ji Woong Kim,[h] Seo Hyoung Chang,[i] Sungmin Woo,[a] Jong-Seong Bae,[j] Sungkyun Park,[h] Young-Min Kim,[cd] Suyoun Lee,[k] Taekjib Choi,[g] Sung Wng Kim[d] and Woo Seok Choi *[a]

Transition metal oxides have been extensively studied and utilized as efficient catalysts. However, the strongly correlated behavior which often results in intriguing emergent phenomena in these materials has been mostly overlooked in understanding the electrochemical activities. Here, we demonstrate a close correlation between the phase transitions and oxygen evolution reaction (OER) in strongly correlated $SrRuO_3$. By systematically introducing Ru–O vacancies into the single-crystalline $SrRuO_3$ epitaxial thin films, we induced a phase transition in crystalline symmetry which resulted in the corresponding modification of the electronic structure. The modified electronic structure significantly affects the electrochemical activities, so a 30% decrease in the overpotential for the OER activity was achieved. Our study suggests that a substantial enhancement in the OER activity can be realized even within single material systems, by rational design and engineering of their crystal and electronic structures.

Broader context

The oxygen evolution reaction (OER) is one of the key electrocatalytic activities, and is utilized in various energy devices, including solid oxide fuel cells and rechargeable batteries. Microscopic understanding of the OER, however, has been rather limited so far. On the other hand, transition metal oxides which often show emergent physical phenomena based on strongly correlated electronic behavior have been extensively studied and utilized as efficient catalysts of the OER. However, the link between strongly correlated behavior and electrocatalytic activity remains elusive. In this communication, we demonstrate a close correlation between the phase transitions in strongly correlated $SrRuO_3$ epitaxial thin films and their OER activity. Using pulsed laser epitaxy, we induced an orthorhombic to tetragonal structural phase transition for the crystalline thin films. The change in crystalline symmetry led to a large modification of the electronic structure, which significantly affected the electrochemical activities. For the tetragonal $SrRuO_3$ thin film, the efficiency of OER activity was enhanced by more than 30% compared to the orthorhombic thin film. Our study suggests that a substantial enhancement in the electrocatalytic activity is possible even within single material systems, by rational design and engineering of their crystal and electronic structures, especially for the strongly correlated transition metal oxides.

Transition metal oxides show promising chemical activities that can be applied in solid oxide fuel cells (SOFCs), rechargeable batteries, catalytic converters, oxygen-separation membranes, and gas sensors.[1–5] The oxygen evolution reaction (OER, $4OH^- \rightarrow O_2 + 2H_2O + 4e^-$) is one of the most important steps in energy conversion and storage mechanisms, and is the efficiency-limiting process in electrolytic water splitting and metal–air batteries.[6,7] The ultimate goal of OER studies is to develop low-cost, highly active, and stable catalysts.[8,9] Recently, perovskite oxides (ABO_3), such as $Ba_{0.5}Sr_{0.5}Co_{0.8}Fe_{0.2}O_{3-\delta}$, $Pr_{0.5}Ba_{0.5}CoO_{3-\delta}$, and $LaCoO_3$, have attracted much attention owing to their intrinsically high OER activity.[10–12] More interestingly, properties such as surface oxygen binding energy, number of outer shell electrons in the transition metal ion, electron occupancy of the e_g orbitals, and the proximity of the oxygen p-band to the Fermi level, have been proposed as descriptors for OER activity.[10,11,13,14] Such approaches, however, have been mainly tested by comparing systems containing different transition metal elements. Unintentionally, such variations in the identity of the elements therein involve commensurate changes in the atomic structures, valence states, electrical resistivities, crystalline surfaces, and overall and specific electronic structures of

[a] *Department of Physics, Sungkyunkwan University, Suwon 16419, Korea. E-mail: choiws@skku.edu*
[b] *Institute of Basic Science, Sungkyunkwan University, Suwon 16419, Korea*
[c] *Center for Integrated Nanostructure Physics, Institute for Basic Science (IBS), Suwon 16419, Korea*
[d] *Department of Energy Sciences, Sungkyunkwan University, Suwon 16419, Korea*
[e] *Materials Modeling and Characterization Department, Korea Institute of Materials Science, Changwon 51508, Korea*
[f] *Department of Physics, Inha University, Incheon 22212, Korea*
[g] *Hybrid Materials Research Center, Department of Nanotechnology and Advanced Materials Engineering, Sejong University, Seoul 05006, Korea*
[h] *Department of Physics, Pusan National University, Busan 46241, Korea*
[i] *Department of Physics, Chung-Ang University, Seoul 06974, Korea*
[j] *Busan Center, Korea Basic Science Institute, Busan 46742, Korea*
[k] *Electronic Materials Research Center, Korea Institute of Science and Technology, Seoul 02792, Korea*

† Electronic supplementary information (ESI) available. See DOI: 10.1039/c7ee00628d

‡ These authors contributed equally to this work.

the materials. Therefore, approaches based on a simplified electronic structure may not apply to distinctive material systems, and a more carefully controlled study, for example, one using a single-material system, is necessary to precisely understand the effect of the catalyst's electronic structure on the OER.[15]

In order to probe the link between the electronic structure and catalytic activity within a single-material system, we exploit the strongly correlated behavior in complex oxides. In particular, the strong coupling among the degrees of freedom of the d-electrons, *i.e.*, charge, spin, orbital, and lattice, in transition metal oxides enables effective tuning of the fundamental physical properties of transition metal oxides.[16,17] In the case of epitaxial thin films, the strong coupling results in a wide spectrum of material properties, which is accessible by tuning epitaxial strain and/or defect concentration. In particular, elemental defects in perovskite oxides can induce modifications in chemical bonding and hybridization between transition metal 3d and oxygen 2p orbitals, which affect the electronic structure significantly. By utilizing these characteristics, we are able to selectively tailor the electronic structure within a single transition metal oxide system.

$SrRuO_3$ (SRO) is a strongly correlated metal that exhibits good OER activity, although it is not very stable in electrochemical environments.[9] Bulk SRO crystals have an orthorhombic structure with lattice parameters of a_o = 5.567, b_o = 5.530, and c_o = 7.845 Å, which can also be represented as a pseudocubic structure with a lattice parameter of a_{pc} = 3.926 Å.[18] Epitaxial SRO thin films exhibit a structural phase transition induced by temperature, epitaxial strain, thickness, and/or vacancy concentration, which makes them suitable for the study of the relationship between fundamental physical properties and OER activities.[19–22] In particular, a structural phase transition to a higher symmetry lattice, *e.g.*, an orthorhombic to tetragonal transition, is observed with increasing entropy (temperature and/or defect concentration) of the system.[19,23]

In this communication, we demonstrate a close correlation between the crystalline symmetry, electronic structure, and OER activity, within the framework of a strongly correlated transition metal (Ru 4d) and oxygen electronic states. In particular, an increase (decrease) in the unoccupied Ru 4d e_g (occupied O 2p) electronic state accompanies an orthorhombic to tetragonal structural transition in epitaxial SRO thin films, which results in a substantial (>30%) decrease in the overpotential for the OER.

In order to induce a phase transition in the crystal structure, we fabricated epitaxial SRO thin films on a single-crystalline $SrTiO_3$ (STO) (001) substrate at different oxygen partial pressures, $P(O_2)$, using pulsed laser epitaxy. Fig. 1 shows the crystal structure of our SRO thin films. The thicknesses of the samples were fixed at ~30 nm (Fig. S1, ESI†). The X-ray diffraction (XRD) θ–2θ scans in Fig. 1(a) represent a monotonic increase of the pseudocubic *c*-axis lattice parameter (c_{pc}) with decreasing $P(O_2)$. The lattice expansion originates from the increased Ru and O vacancies with decreasing $P(O_2)$, as will be discussed later in more detail. Despite the introduction of elemental vacancies, all the SRO thin films are coherently strained to the STO substrate, as exemplified in the reciprocal space map around the (103) STO Bragg reflection, shown in Fig. 1(b). All the thin films show good crystallinity, as indicated by the peaks in the rocking curve scans, with full-width-at-half-maximum (FWHM) values of <0.02° (Fig. S2, ESI†).

We observed an orthorhombic to tetragonal structural phase transition with a decrease in $P(O_2)$ for our fully strained epitaxial SRO thin films. In particular, XRD off-axis θ–2θ scans show a

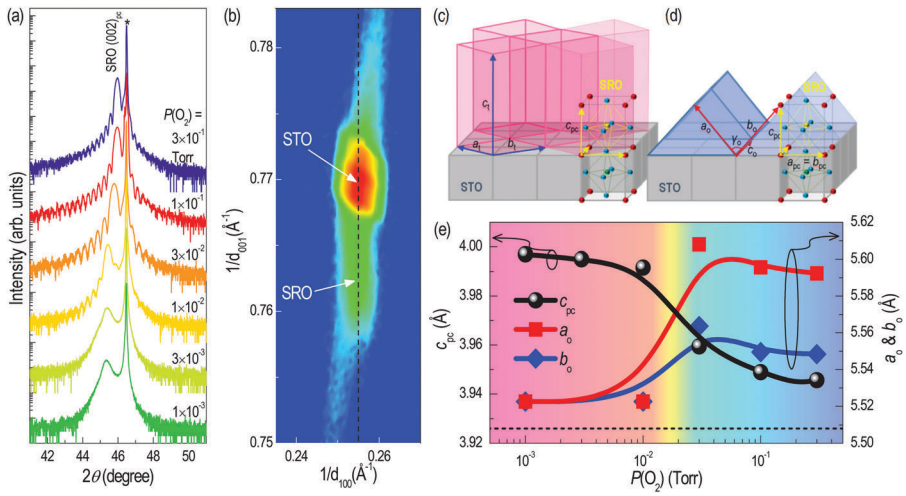

Fig. 1 Elemental vacancy induced structural phase transition in epitaxially strained $SrRuO_3$ thin films. (a) XRD θ–2θ scans for epitaxial $SrRuO_3$ thin films grown at different $P(O_2)$ around the (002) Bragg reflections of the $SrTiO_3$ substrates (*). With decreasing $P(O_2)$, the $(002)_{pc}$ peak of $SrRuO_3$ shifts to a lower angle, indicating an increase of the c_{pc}-axis lattice constant. (b) XRD reciprocal space map of the $SrRuO_3$ thin film grown at $P(O_2) = 10^{-1}$ Torr around the (103) Bragg reflection of the $SrTiO_3$ substrate, which shows a coherently strained film without any lattice relaxation. Schematic diagrams of (c) tetragonal and (d) orthorhombic $SrRuO_3$ thin films epitaxially grown on $SrTiO_3$ substrates. The lattice parameters are redefined according to the crystal symmetry for each structure. (e) Evolution of the orthorhombic and pseudocubic lattice constants of epitaxial $SrRuO_3$ thin films as a function of $P(O_2)$. A clear structural phase transition is observed at $P_c(O_2) = \sim 2 \times 10^{-2}$ Torr. The pseudocubic lattice constant of bulk $SrRuO_3$ (c_{pc} = 3.926 Å, black dashed line) is shown for comparison. Background colors represent the tetragonal (red) and orthorhombic (blue) phase regions.

clear distinction between the films grown at $P(O_2) \geq 3 \times 10^{-2}$ and $\leq 1 \times 10^{-2}$ Torr (Fig. S3, ESI†).[23–26] Fig. 1(e) summarizes the calculated lattice parameters for the epitaxial SRO thin films grown at varying $P(O_2)$ obtained by the above XRD analyses (Table S1, ESI†). An abrupt change in the orthorhombic lattice parameters is observed across $P_c(O_2) = \sim 2 \times 10^{-2}$ Torr, which is the critical $P(O_2)$ for the structural phase transition. Consequently, crystal structures for the epitaxial SRO thin films are schematically shown in Fig. 1(c) and (d), *i.e.*, a distorted orthorhombic structure (Fig. 1(d)) for the films grown at $P(O_2) > P_c(O_2)$ and a tetragonal structure (Fig. 1(c)) for the films grown at $P(O_2) < P_c(O_2)$, within the preserved perovskite framework. (The lattice parameters are redefined according to the crystal symmetry for each structure.)

The $P(O_2)$-dependent orthorhombic-to-tetragonal phase transition is driven by the increased elemental vacancy concentrations within the SRO epitaxial thin films. We performed X-ray photoelectron spectroscopy (XPS), which confirms a systematic and gradual increase of the Ru and O vacancies with decreasing $P(O_2)$. While it is technically difficult to determine the exact stoichiometry of oxide thin films, we can understand the qualitative trend of the vacancy formation. Fig. 2(a) and (b) show Ru 3d with an asymmetric peak shape and O 1s core level photoemission spectra, respectively. The peaks at binding energies of 285.5, 281.4, and 529.0 eV correspond to Ru $3d_{3/2}$, $3d_{5/2}$ (spin–orbit splitting of 4.1 eV), and O 1s orbitals, respectively.[27] From the XPS spectra we clearly observe a systematic decrease in the Ru 3d spin–orbit doublets and an increase in the O vacancy states with decreasing $P(O_2)$.[28] Fig. 2(c) shows the relative atomic concentration of each element in the thin films, obtained from the spectral weight of the deconvoluted peaks. With decreasing $P(O_2)$, a continuous decrease in Ru and O concentrations is observed, along with an increase in O vacancy concentration (V_O) and the secondary phase (Sr–O). Interestingly, the elemental vacancy concentrations do not show a drastic increase across $P_c(O_2)$. Hence, the structural phase transition is not induced by abrupt changes in the vacancy concentrations. Instead, despite a small difference, when a critical amount of elemental vacancies is introduced, the energy of sustaining the orthorhombic structure becomes too high and the structure lowers the energy by transforming into a tetragonal structure. Theoretical calculation of the vacancy formation energy further supports the elemental vacancy engineering of the crystal structure (Table S2, ESI†).

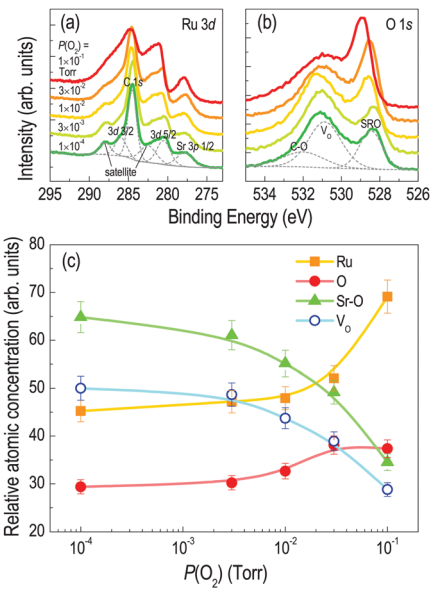

Fig. 2 Elemental defect concentration in $SrRuO_3$ thin films by X-ray photoelectron spectroscopy. (a) Ru 3d core-level and (b) O 1s XPS spectra of the $SrRuO_3$ thin films grown at different $P(O_2)$. The spectra are vertically shifted for clarity. Starting from stoichiometric $SrRuO_3$, an increase of Ru and O vacancies is shown with decreasing $P(O_2)$. (c) Relative atomic concentration in $SrRuO_3$ thin films, showing a systematic increase of Ru and O vacancies with decreasing $P(O_2)$. While the crystal structure of the $SrRuO_3$ thin films shows a clear phase transition at $P_c(O_2) = \sim 2 \times 10^{-2}$ Torr, the Ru and O vacancy concentrations do not show such an abrupt change.

Concomitant with the structural phase transition, we observed a substantial modification of the electronic structure of SRO thin films across $P_c(O_2)$. Fig. 3 shows the optical spectroscopic results obtained by spectroscopic ellipsometry, which reflects the electronic structure near the Fermi level. The real part of the optical conductivity spectra, $\sigma_1(\omega)$ (Fig. 3(a)), clearly exhibits the evolution of optical transitions by changing $P(O_2)$, especially across the structural phase transition. SRO thin films typically show a Drude absorption at low photon energy, indicating metallic behavior. In addition, four different peaks, labelled as α, A, β, and B at ~1.7, ~3.3, ~4.1, and ~6.2 eV, are attributed to Ru 4d $t_{2g} \rightarrow t_{2g}$, O 2p → Ru 4d t_{2g}, Ru 4d $t_{2g} \rightarrow e_g$, and O 2p → Ru 4d e_g optical transitions, respectively.[29,30] In particular, the optical transition peaks A and B directly represent the quantitative hybridization strength between the Ru and O states. In order to extract the individual parameters for each optical transition, we used the following Drude–Lorentz analysis:

$$\sigma_1(\omega) = \frac{e^2}{m^*}\frac{n_D\gamma_D}{\omega^2+\gamma_D^2} + \frac{e^2}{m^*}\sum_j \frac{n_j\gamma_j\omega^2}{\left(\omega_j^2-\omega^2\right)^2+\gamma_j^2\omega^2}, \quad (1)$$

where e, m^*, n_j, γ_j, and ω_j are the electronic charge, effective mass, carrier density, scattering rate, and resonant frequency of the j-th oscillator, respectively. The first term describes the coherent Drude response from free charge carriers (subscript D), and the second term describes the optical transitions from occupied to unoccupied electronic states. Although the position (ω_j) and the width (γ_j) of the optical transition peaks do not change significantly, a strong redistribution of the spectral weight ($W_s \equiv \int \sigma_j(\omega)d\omega \propto n_j/\omega_j^2$) is observed with decreasing $P(O_2)$, as shown in Fig. 3(b). In particular, with increasing Ru–O vacancy concentrations, W_{sB} and $W_{s\beta}$ show an abrupt decrease and increase, respectively, across the structural phase transition. $W_{s\beta}$ even surpasses W_{sA} for the tetragonal phase SRO thin films, indicating a strong modification of the electronic structure.

The abrupt change in the electronic structure can be understood by considering the crystal structure as well as the elemental vacancy concentration. First, we note that both A and B are charge transfer transitions involving an occupied O 2p state. Therefore, the transition probabilities (W_{sA} and W_{sB}) might decrease as more O vacancies are introduced with decreasing $P(O_2)$. It also indicates that the hybridization strength between the Ru and O states is

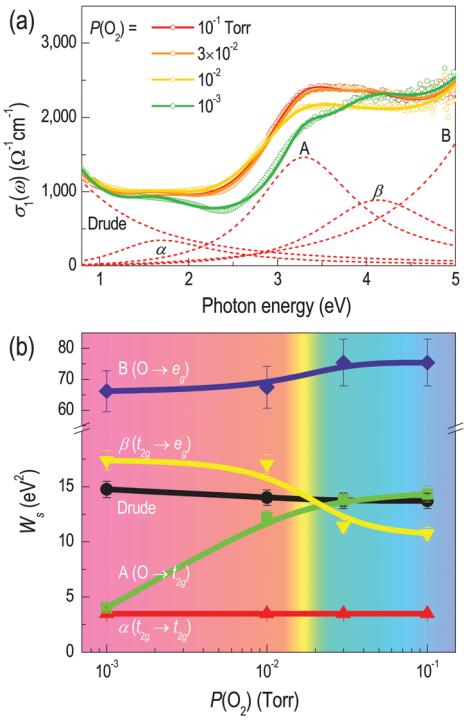

Fig. 3 Elemental defect induced electronic structure transition in $SrRuO_3$ thin films. (a) Real part of the optical conductivity, $\sigma_1(\omega)$, of the $SrRuO_3$ thin films. The symbols denote the experimental spectra and the lines represent the Drude–Lorentz fitting results. The optical transitions at ~1.7, ~3.1, ~4.4, and ~6.2 eV are assigned to peaks α, A, β, and B, respectively. The transitions correspond to d–d transition between Ru 4d t_{2g} states (α), d–d transition between Ru 4d t_{2g} and e_g states (β), charge transfer transition between O 2p and Ru 4d t_{2g} states (A), and charge transfer transition between O 2p and Ru 4d e_g states (B). The dashed lines represent the deconvoluted Lorentzian peaks corresponding to each characteristic optical transition. (b) Spectral weight (W_s) evolution of the Lorentz oscillators as a function of $P(O_2)$. With decreasing $P(O_2)$, W_{sA} and W_{sB} decrease, while $W_{s\beta}$ increases. In particular, W_s for most transitions shows an abrupt change at $P_c(O_2)$ = ~2×10^{-2} Torr, indicating a transition in the electronic structure.

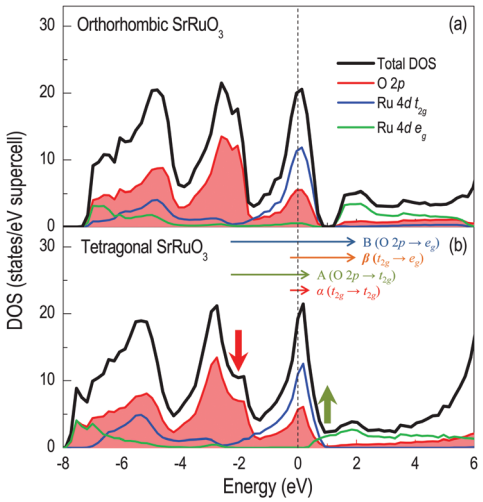

Fig. 4 Density of states (DOS) of (a) orthorhombic and (b) tetragonal $SrRuO_3$. The density of states indicates a decrease in the occupied O 2p band and an enhancement of the unoccupied Ru 4d e_g band as the structure changes from orthorhombic to tetragonal. The horizontal arrows indicate the optical transitions observed in Fig. 3. The change in the theoretical electronic structure owing to the phase transition coincides with the change in the experimental optical spectra.

substantially decreased as the crystal structure changes into a tetragonal structure. In addition, the increase in $W_{s\beta}$ can be understood in terms of the Ru–O–Ru bond angle. As the crystal structure undergoes a phase transition from orthorhombic to tetragonal at $P_c(O_2)$, the Ru–O–Ru bond angle approaches 180°, facilitating inter-site d–d transitions due to the greater overlap of 4d orbitals. Conversely, $W_{s\alpha}$ shows little, if any, $P(O_2)$ dependence, since the bond angle dependence will be weaker for the t_{2g} orbitals compared to the elongated e_g orbitals that are responsible for the transition β. The more abrupt nature of W_{sB} compared to W_{sA} can also be explained by the involvement of the unoccupied e_g orbital.

With the help of density functional theory calculation, we can further confirm that the electronic structure transition is predominantly associated with the crystal symmetry change. Fig. 4 shows the electronic density of states of the orthorhombic and tetragonal SRO. The overall features of the two phases are quite similar, reproducing all the expected optical transitions as indicated by the horizontal arrows in Fig. 4(a). Moreover, the essential differences in the predicted electronic structure are clearly observed, as indicated by the vertical arrows in Fig. 4(b). For the tetragonal SRO, the occupied O 2p level (near −2 eV) is suppressed, while the unoccupied Ru 4d e_g level (near 1 eV) is enhanced. In particular, the increase of the unoccupied e_g level, or closing of the energy gap around 1 eV, in the tetragonal SRO is closely related to the octahedral distortion in the orthorhombic structure, as previously discussed. Indeed, it has been shown that octahedral rotation leads to gap opening in 4d transition metal oxides, including Sr_2RuO_4.[31,32] It should be further noted that the elemental vacancies do not significantly contribute to the changes in the density of states when compared to the contribution made by the structural transition. Fig. S4 (ESI†) shows the effect of RuO vacancies in determining the electronic structure of the tetragonal SRO thin films, which is relatively weak compared to the effect of the structural transition. (The main changes denoted by the vertical arrows are undisturbed by introducing vacancies.)

The modification of the electronic structure in the epitaxial SRO thin films influences the electrochemical activity significantly. Fig. 5 shows the current density as a function of potential with reference to a reversible hydrogen electrode (RHE) for the SRO thin films in KOH solution. Our cyclic voltammetry data for the orthorhombic SRO thin film ($P(O_2) \geq 3 \times 10^{-2}$ Torr) show good agreement with a recent study on epitaxial SRO thin films. Chang *et al.* described the current enhancement in the cyclic voltammetry mainly due to the OER activity in SRO, separately confirmed by rotating ring disk electrode (RRDE) experiments on Ru metal.[9] Furthermore, a lower onset potential value (<1.25 V) has been observed in our tetragonal SRO, which is close to the calculated thermodynamic equilibrium potential value (1.23 V).[14] The extremely low overpotential allows us to consider partial contribution from a transient anodic current based on the

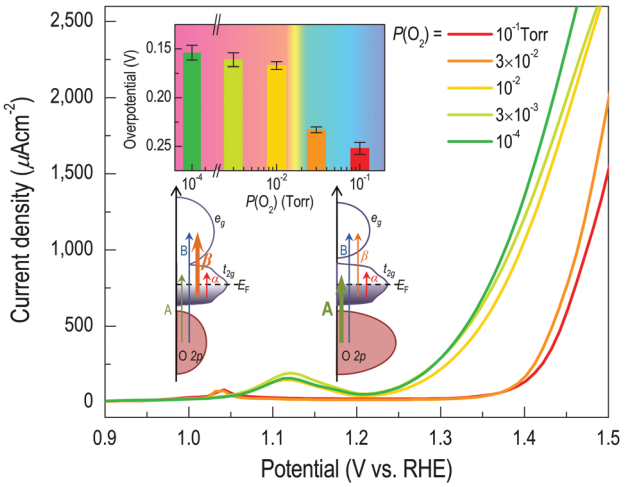

Fig. 5 Catalytic OER effect of $SrRuO_3$ thin films with elemental vacancies. Current–potential curves during the first potential sweep for the OER on SRO thin film electrodes in a 1 M KOH electrolyte. As the $P(O_2)$ decreases from 10^{-1} to 10^{-4} Torr, the overpotential also decreases. The insets show the overpotential at the current density of 1000 μA cm^{-2} as a function of $P(O_2)$. Schematic band diagrams are also shown for the tetragonal (larger Ru 4d e_g state) and the orthorhombic (larger O 2p state) structures of epitaxial SRO thin films.

oxidation of the SRO thin film itself. However, from cyclic voltammetry at low potential, XRD, XPS, inductively coupled plasma-mass spectroscopy (ICP-MS), and chronoamperometric measurements, we confirmed that both orthorhombic and tetragonal SRO thin films are stable at least up to 1.3 V, which is well above the onset potential of OER (Fig. S8–S12, ESI†). Although more transient behavior due to the dissolution of the material could be observed as we further increased the potential, such behavior did not occur at a low potential range.

The OER behavior can be clearly distinguished between the orthorhombic and tetragonal SRO thin films. The cyclic voltammetry curves can be easily categorized into two groups, *i.e.*, the tetragonal SRO thin films exhibit a lower onset potential, indicating a higher OER activity, compared to the orthorhombic SRO thin films. These results clearly demonstrate that the crystal and/or electronic phase transition is responsible for the remarkably enhanced OER activity, on top of the more gradual improvements possibly due to vacancy incorporation in the thin films. In addition, we have observed a reproducible pre-peak in the cyclic voltammetry below the onset of the OER. While its exact origin is not currently understood,[33,34] the pre-peak is specific for the orthorhombic (~1.12 V) and tetragonal (~1.04 V) SRO thin film catalysts, further suggesting a correlation between the electronic structure and catalytic activity. The inset of Fig. 5 shows that the overpotential for the film grown at high $P(O_2)$ (3×10^{-2} Torr) is 0.233 V, while that for the film grown at low $P(O_2)$ (1×10^{-2} Torr) is 0.154 V. Therefore, a 30% reduction in the overpotential is achieved with the concomitant structural and electronic phase transitions in SRO thin films.

We provide further experimental evidence to support that the significant decrease in the overpotential is due to the change in the electronic structure. First, we provide the electrical resistivity as a function of temperature (Fig. S5, ESI†). Interestingly, the resistivity increases with increasing defect concentration (decreasing $P(O_2)$), which is the opposite trend to the increasing current density observed in the alkaline solution. Therefore, the decrease in the overpotential for the tetragonal SRO in KOH solution cannot be attributed to a more conducting sample, and is indeed due to the enhanced chemical activity. Second, the orthorhombic and tetragonal SRO epitaxial thin films show a comparable structural and surface quality, as shown in Fig. S2 (ESI†). The rocking curve scan indicates the excellent crystallinity of the samples, and the atomic force microscopy (AFM) topography images show the single unit cell step-and-terrace structure of the substrate, which is well-preserved even after the thin-film growth, for the samples grown just above and below $P_c(O_2)$. The rms roughness values obtained from the topographic images are also comparable. The XRD θ–2θ scans also show prominent thickness fringes for the SRO films grown down to $P(O_2) = 1 \times 10^{-2}$ Torr, which is below $P_c(O_2)$, indicating that the surface structural quality is not the main factor for the enhancement of the OER activity in the tetragonal SRO thin films. Moreover, since we do not observe any abrupt increase in the Ru and O vacancy concentrations (Fig. 2), the modification of the electronic structure is the best natural explanation for the enhanced catalytic activity in the tetragonal SRO thin films.

The simplified schematic band diagrams in the inset of Fig. 5 illustrate the essential modification of the electronic structure that should be associated with the change in the observed electrochemical activity. We specifically note that the hybridization strength between the Ru and O states within the SRO thin films can substantially influence the OER activity. Indeed, metal–oxygen hybridization in 3d transition metal oxides has been recently proposed as an important factor in determining the electrocatalytic activity.[3,35,36] The mechanism of OER in alkaline solution consists of a series of elementary electron-transfer steps, the efficiencies of which are determined by the creation and breaking of chemical bonds between the adsorbate molecules such as O*, OO*, OH*, and OOH* and the surface transition metal ions.[37,38] As the A peak in optical spectroscopy is a straightforward measure of the hybridization strength, the tetragonal SRO thin film has a lower hybridization strength compared to the orthorhombic thin film. The reduced hybridization within the RuO_6 octahedra can facilitate the formation of the chemical bonding between the Ru and the adsorbate molecules. In addition, the increase in the unoccupied e_g state might indicate the easier formation of a more oxidized (unstable) active Ru site, which could further facilitate the activity.[9]

A recent scanning tunneling microscopy study also underscored the important role of the RuO_6 octahedra in understanding water molecule adsorption at the ruthenate surfaces.[39] In particular, the structural flexibility or "rigidity" of the octahedra in perovskite oxides was identified as the key factor influencing molecular adsorption. The exact difference between the orthorhombic and tetragonal SRO surfaces at the molecular level is yet to be discovered, in terms of the difference in bonding character and possible surface superstructures. Nevertheless,

the effect of structural and electronic modification on the surface chemistry and reactivity in a single-material system has been clearly demonstrated.

Conclusions

In conclusion, we have studied the close correlation between the crystalline symmetry, electronic structure, and OER activity of single-crystalline $SrRuO_3$ thin films. A critical oxygen partial pressure of $\sim 2 \times 10^{-2}$ Torr during the pulsed laser epitaxial growth clearly divided the grown epitaxial thin films into two groups, *i.e.*, orthorhombic and tetragonal phases for high and low pressure growth, respectively. The elemental-vacancy-induced phase transition in the crystalline lattice accompanied a change in the electronic structure. The modification of the electronic structure affected the electrocatalytic activity substantially, reducing the overpotential of the OER by more than 30%. Our approach provides an effective framework for discovering an appropriate descriptor for different chemical activities and can be applied to other strongly correlated transition metal oxide catalysts.

Acknowledgements

S. A L. and S. O. contributed equally to this work. We thank Janice L. Musfeldt, Changyoung Kim, and S. S. Ambrose Seo for valuable discussions. We appreciate S.-J. Park for her help on 2D-RSM measurement at Korea ITS Co. Ltd. This work was supported by Basic Science Research Programs through the National Research Foundation of Korea (NRF) (NRF-2014R1A2A2A01006478, NRF-2016R1A6A3A11934867 (S. A L.), NRF-2015R1C1A1A02037595 (M. C.), NRF-2015R1C1A1A01053163 (S. H. C.), and NRF-2015R1D1A1A01058672 (S. P.)), and NRF-2014R1A1A006405 (T. C.). S. L. was supported by the Korea Institute of Science and Technology (KIST) through 2E25800. This work was also supported by IBS-R011-D1.

Notes and references

1 P. Simon and Y. Gogotsi, *Nat. Mater.*, 2008, **7**, 845–854.
2 P. G. Bruce, S. A. Freunberger, L. J. Hardwick and J.-M. Tarascon, *Nat. Mater.*, 2012, **11**, 19–29.
3 J. Suntivich, H. A. Gasteiger, N. Yabuuchi, H. Nakanishi, J. B. Goodenough and Y. Shao-Horn, *Nat. Chem.*, 2011, **3**, 546–550.
4 F. Cheng and J. Chen, *Chem. Soc. Rev.*, 2012, **41**, 2172–2192.
5 C. D. Lokhande, D. P. Dubal and O.-S. Joo, *Curr. Appl. Phys.*, 2011, **11**, 255–270.
6 H. Dau, C. Limberg, T. Reier, M. Risch, S. Roggan and P. Strasser, *ChemCatChem*, 2010, **2**, 724–761.
7 M. W. Kanan and D. G. Nocera, *Science*, 2008, **321**, 1072–1075.
8 D. Chen, C. Chen, Z. M. Baiyee, Z. Shao and F. Ciucci, *Chem. Rev.*, 2015, **115**, 9869–9921.
9 S. H. Chang, N. Danilovic, K. C. Chang, R. Subbaraman, A. P. Paulikas, D. D. Fong, M. J. Highland, P. M. Baldo, V. R. Stamenkovic, J. W. Freeland, J. A. Eastman and N. M. Markovic, *Nat. Commun.*, 2014, **5**, 4191.
10 J. Suntivich, K. J. May, H. A. Gasteiger, J. B. Goodenough and Y. Shao-Horn, *Science*, 2011, **334**, 1383–1385.
11 A. Grimaud, K. J. May, C. E. Carlton, Y. L. Lee, M. Risch, W. T. Hong, J. G. Zhou and Y. Shao-Horn, *Nat. Commun.*, 2013, **4**, 7.
12 K. A. Stoerzinger, W. S. Choi, H. Jeen, H. N. Lee and Y. Shao-Horn, *J. Phys. Chem. Lett.*, 2015, **6**, 487–492.
13 J. O. M. Bockris and T. Otagawa, *J. Electrochem. Soc.*, 1984, **131**, 290–302.
14 I. C. Man, H.-Y. Su, F. Calle-Vallejo, H. A. Hansen, J. I. Martínez, N. G. Inoglu, J. Kitchin, T. F. Jaramillo, J. K. Nørskov and J. Rossmeisl, *ChemCatChem*, 2011, **3**, 1159–1165.
15 Z. Lu, H. Wang, D. Kong, K. Yan, P.-C. Hsu, G. Zheng, H. Yao, Z. Liang, X. Sun and Y. Cui, *Nat. Commun.*, 2014, **5**, 4345.
16 J. M. Rondinelli and N. A. Spaldin, *Adv. Mater.*, 2011, **23**, 3363–3381.
17 H. Y. Hwang, Y. Iwasa, M. Kawasaki, B. Keimer, N. Nagaosa and Y. Tokura, *Nat. Mater.*, 2012, **11**, 103–113.
18 C. W. Jones, P. D. Battle, P. Lightfoot and W. T. A. Harrison, *Acta Crystallogr., Sect. C: Cryst. Struct. Commun.*, 1989, **45**, 365–367.
19 W. L. Lu, P. Yang, W. D. Song, G. M. Chow and J. S. Chen, *Phys. Rev. B: Condens. Matter Mater. Phys.*, 2013, **88**, 214115.
20 K. J. Choi, S. H. Baek, H. W. Jang, L. J. Belenky, M. Lyubchenko and C.-B. Eom, *Adv. Mater.*, 2010, **22**, 759–762.
21 D. Kan, R. Aso, H. Kurata and Y. Shimakawa, *J. Appl. Phys.*, 2013, **113**, 173912.
22 A. T. Zayak, X. Huang, J. B. Neaton and K. M. Rabe, *Phys. Rev. B: Condens. Matter Mater. Phys.*, 2006, **74**, 094104.
23 W. Lu, W. D. Song, K. He, J. Chai, C.-J. Sun, G.-M. Chow and J.-S. Chen, *J. Appl. Phys.*, 2013, **113**, 063901.
24 S. H. Chang, Y. J. Chang, S. Y. Jang, D. W. Jeong, C. U. Jung, Y. J. Kim, J. S. Chung and T. W. Noh, *Phys. Rev. B: Condens. Matter Mater. Phys.*, 2011, **84**, 104101.
25 D. Kan and Y. Shimakawa, *Cryst. Growth Des.*, 2011, **11**, 5483–5487.
26 A. Vailionis, H. Boschker, W. Siemons, E. P. Houwman, D. H. A. Blank, G. Rijnders and G. Koster, *Phys. Rev. B: Condens. Matter Mater. Phys.*, 2011, **83**, 064101.
27 J. Shin, S. V. Kalinin, H. N. Lee, H. M. Christen, R. G. Moore, E. W. Plummer and A. P. Baddorf, *Surf. Sci.*, 2005, **581**, 118–132.
28 J. C. C. Fan and J. B. Goodenough, *J. Appl. Phys.*, 1977, **48**, 3524–3531.
29 J. S. Lee, Y. S. Lee, T. W. Noh, K. Char, J. Park, S. J. Oh, J. H. Park, C. B. Eom, T. Takeda and R. Kanno, *Phys. Rev. B: Condens. Matter Mater. Phys.*, 2001, **64**, 245107.
30 D. W. Jeong, H. C. Choi, C. H. Kim, S. H. Chang, C. H. Sohn, H. J. Park, T. D. Kang, D.-Y. Cho, S. H. Baek, C. B. Eom, J. H. Shim, J. Yu, K. W. Kim, S. J. Moon and T. W. Noh, *Phys. Rev. Lett.*, 2013, **110**, 247202.
31 B. J. Kim, J. Yu, H. Koh, I. Nagai, S. I. Ikeda, S. J. Oh and C. Kim, *Phys. Rev. Lett.*, 2006, **97**, 106401.

32 E. Ko, B. J. Kim, C. Kim and H. J. Choi, *Phys. Rev. Lett.*, 2007, **98**, 226401.
33 N. Danilovic, R. Subbaraman, K. C. Chang, S. H. Chang, Y. J. Kang, J. Snyder, A. P. Paulikas, D. Strmcnik, Y. T. Kim, D. Myers, V. R. Stamenkovic and N. M. Markovic, *Angew. Chem., Int. Ed.*, 2014, **53**, 14016–14021.
34 M. Wohlfahrt-Mehrens, J. Schenk, P. M. Wilde, E. Abdelmula, P. Axmann and J. Garche, *J. Power Sources*, 2002, **105**, 182–188.
35 J. Suntivich, W. T. Hong, Y.-L. Lee, J. M. Rondinelli, W. Yang, J. B. Goodenough, B. Dabrowski, J. W. Freeland and Y. Shao-Horn, *J. Phys. Chem. C*, 2014, **118**, 1856–1863.
36 R. G. Hadt, D. Hayes, C. N. Brodsky, A. M. Ullman, D. M. Casa, M. H. Upton, D. G. Nocera and L. X. Chen, *J. Am. Chem. Soc.*, 2016, **138**, 11017–11030.
37 B. Hammer and J. K. Nørskov, *Theoretical surface science and catalysis—calculations and concepts*, Academic Press, 2000.
38 J. Rossmeisla, Z.-W. Qub, H. Zhub, G.-J. Kroesb and J. K. Nørskov, *J. Electroanal. Chem.*, 2007, **607**, 83–89.
39 D. Halwidl, B. Stoger, W. Mayr-Schmolzer, J. Pavelec, D. Fobes, J. Peng, Z. Q. Mao, G. S. Parkinson, M. Schmid, F. Mittendorfer, J. Redinger and U. Diebold, *Nat. Mater.*, 2016, **15**, 450–455.

